PNAS RESEARCH ARTICLE | PLANT BIOLOGY

# AtFH5 recruits and transports the arabinogalactan protein AGP23 to maintain the tip growth of pollen tube

Jiang Li[a,b], Ligang Fan[a,b], Ting Yang[a,b], Puzhi Zhang[a,b], Huaqiang Ruan[a,b], Yihao Li[b], Ting Wang[a], Yi Zhang[a], Fanfan Zhang[a,1], and Haiyun Ren[a,b,1]

Affiliations are included on p. 10.

Edited by Zhenbiao Yang, Chinese Academy of Sciences Shenzhen Institutes of Advanced Technology, Shenzhen, China; received May 28, 2024; accepted October 9, 2024 by Editorial Board Member Joseph J. Kieber

**Actin cytoskeleton drives the targeted transport of cell wall components to sustain the tip growth of pollen tubes for double fertilization; however, the underlying mechanism remains largely unknown. *Arabidopsis* formin 5 (AtFH5), an actin-nucleating protein, localizes at secretory vesicles and mediates actin polymerization-based vesicle trafficking in pollen. Here, we demonstrate that AtFH5 determines the recruitment and transport of cell wall components in AtFH5-labeled vesicles during the tip growth of pollen tubes. Through a screen of interacting proteins of AtFH5, we identify many cell wall–related proteins, with arabinogalactan protein 23 (AGP23) occupying the highest frequency. AtFH5 interacts with AGP23 via its N-terminal extracellular domain (ECD) and jointly regulate the pollen germination and tube growth process. Further observations reveal that AGP23 co-localizes with AtFH5 at moving vesicles, germination sites, and pollen tube tips, suggesting that AGP23 is delivered by AtFH5-labeled vesicles. Deletion of the ECD of AtFH5 interrupts the dynamic localization and cell-wall connection of AGP23 in pollen grains and tubes. Cytological and genetic evidence shows that AGP23 and AtFH5 work in the same pathway to modulate cell wall composition. Together, our data uncover a role of formin in directing the sorting and deposition of cell wall components via secretory vesicle trafficking during pollen germination and tube growth.**

pollen | tip growth | cell wall | AtFH5 | AGP23

## Significance

Targeted transport and deposition of cell wall components to the growing point are essential for pollen tube growth. Arabinogalactan proteins (AGPs) are multifunctional glycoproteins of the plant cell wall; yet the mechanism underlying their delivery to the cell wall and how this process affects pollen tube growth remain elusive. *Arabidopsis* formin 5 (AtFH5) mediates actin polymerization at secretory vesicles to promote a self-propulsion mode of vesicle trafficking in pollen. Here, we reveal that AtFH5 recruits AGPs into its vesicles and steers the transport of itself and AGPs to the plasma membrane-cell wall destination during pollen germination and tube growth. This study provides insights into intracellular sorting and trafficking of cell wall materials from a cytoskeletal perspective.

Pollen germination and pollen tube elongation are essential steps for double fertilization in flowering plants. To guarantee the rapid growth of pollen tubes, it requires a steady stream of new materials to be directionally transported to the tip of pollen tube and properly positioned at the growing point (1–3). Actin cytoskeleton plays a critical role in regulating secretory vesicle trafficking in pollen (4–7); however, how actin cytoskeleton modulates the transport of cell wall components remains elusive (8–10).

*Arabidopsis* formin 5 (AtFH5), a transmembrane actin-nucleating protein, belongs to the class I family of formins (11). Previous researches show that AtFH5 localizes at secretory vesicles and mediates actin polymerization via its C-terminal Formin Homology domains (FH1 and FH2) to drive a self-propelling movement of vesicles during pollen germination (12–14); just before germination, AtFH5 transfers to the plasma membrane (PM) at the prospective germination site and directs the polarity establishment of pollen grains (12, 13); during pollen tube growth, AtFH5 is persistently targeted to the vesicles, PM, and cell wall at the apical dome of pollen tube (15, 16). However, little is known regarding which substances are transported by AtFH5-labeled vesicles and how these substances are selected into these vesicles.

While studies on formins have long been focused on the actin nucleating activity of FH1 and FH2 domains, a few reports recently revealed the functional significance of their N-terminal domains. The *Arabidopsis* formin 1 (AtFH1) and *Medicago truncatula* symbiotic formin 1 are thought to be anchored within the PM by the cell wall connection mediated by their extracellular domains (ECDs) (17, 18). AtFH3 and AtFH5 have distinct localization patterns in pollen tube, but the replacement of the N-terminal of AtFH3 with that of AtFH5 mimics the localization of wild-type (WT) AtFH5 (16). The different glycosylation modifications in their ECDs may cause the different localization of AtFH3 and AtFH5 (19). These data imply that the cell wall association involved by the ECD of AtFH5 is necessary for its PM localization in pollen tube (16–19). But the interacting factor of AtFH5 on the cell wall side remains unknown and the specific biological function of the N-terminal of AtFH5 still needs further investigations.

Arabinogalactan proteins (AGPs), consisting of a hydroxyproline-rich protein backbone and one or more arabinose or galactose-rich glycan side chains, are a class of glycoproteins

Author contributions: H. Ren and J.L. designed research; J.L., L.F., T.Y., P.Z., and H. Ruan performed research; L.F., T.Y., P.Z., H. Ruan, and Y.L. contributed new reagents/analytic tools; J.L., T.W., Y.Z., F.Z., and H. Ren analyzed data; and F.Z. and H. Ren wrote the paper.

The authors declare no competing interest.

This article is a PNAS Direct Submission Z.Y. is a guest editor invited by the Editorial Board.



[1]To whom correspondence may be addressed. Email: ffzhang@bnu.edu.cn or hren@bnu.edu.cn.

This article contains supporting information online at https://www.pnas.org/lookup/suppl/doi:10.1073/pnas.2410607121/-/DCSupplemental.

Published November 25, 2024.

ubiquity in plants (20–22). They are processed via the secretory pathway and are ultimately delivered to the cell wall or to the extracellular face of the PM through secretory vesicles (23, 24). AGPs are proposed to be fundamental players in plant growth and development, particularly in sexual reproduction (21, 22, 25–27). The stylar transmitting tissue-specific AGPs in *Nicotiana tabacum*, called transmitting tissue-specific protein, stimulated pollen tube growth in vivo and were required for pollen tube guidance (28, 29). Early pharmacological experiments showed that pollen germination and tube growth were inhibited after the treatment of β-Yariv reagent, which specifically binds to and inactivates AGPs (20). Some AGP-specific antibodies also strongly label pollen germination sites and tube tips (30). AGP6, AGP11, AGP23, and AGP40 are pollen-specific AGPs, and the *Arabidopsis agp6 agp11* double mutant displayed abnormal pollen germination as well as pollen tube growth (31–33). These data reveal a critical role of AGPs for pollen germination and tube growth. So far, however, the molecular mechanism by which AGPs are recruited and transported to cell wall and how this process affects pollen germination and tube growth remains unknown.

In this study, we identify a function of AtFH5 that recruits the cell wall component AGP23 to sustain pollen germination and tube growth. The transport and proper positioning of AGP23 in pollen grains and tubes require the ECD of AtFH5. This study reveals that AtFH5 are required for sorting and transporting cell wall materials, which will enhance our understanding of how formins function in pollen.

## Results

**The N-Terminal of AtFH5 Interacts with an Arabinogalactan Protein AGP23.** To fully elucidate the function of AtFH5 in pollen, we performed a yeast-two-hybrid (Y2H) screen using AtFH5 as the bait in a complementary DNA (cDNA) library of *Arabidopsis* mature pollens. From this screen, we totally identified 44 candidates, and many of them are cell wall related proteins (*SI Appendix*, Fig. S1*A* and Table S1). We found some AGPs in this screen (*SI Appendix*, Table S1). Further point-to-point Y2H and split-luciferase complementation assays (LCA) demonstrated that AtFH5 interacted with all of these pollen-specific AGPs (including AGP6, AGP11, AGP23, and AGP40) (*SI Appendix*, Fig. S1 *B* and *C*). As AGP23 occupied the highest frequency during this screening (*SI Appendix*, Fig. S1*D*), we focused on the interplay between AtFH5 and AGP23. A domain analysis of AtFH5 identified that a signal peptide (SP), a proline-rich ECD, a transmembrane domain (TM), a variable domain (VD), a FH1 domain, and a FH2 domain, are sequentially arranged from the N-terminal to the C-terminal (Fig. 1*A*). The ECD of AtFH5 possess a high content of proline residues with repetitive Ser-$Pro_{(3\text{-}5)}$ (extensin, EXT) motifs required for glycosylation (19, 34)

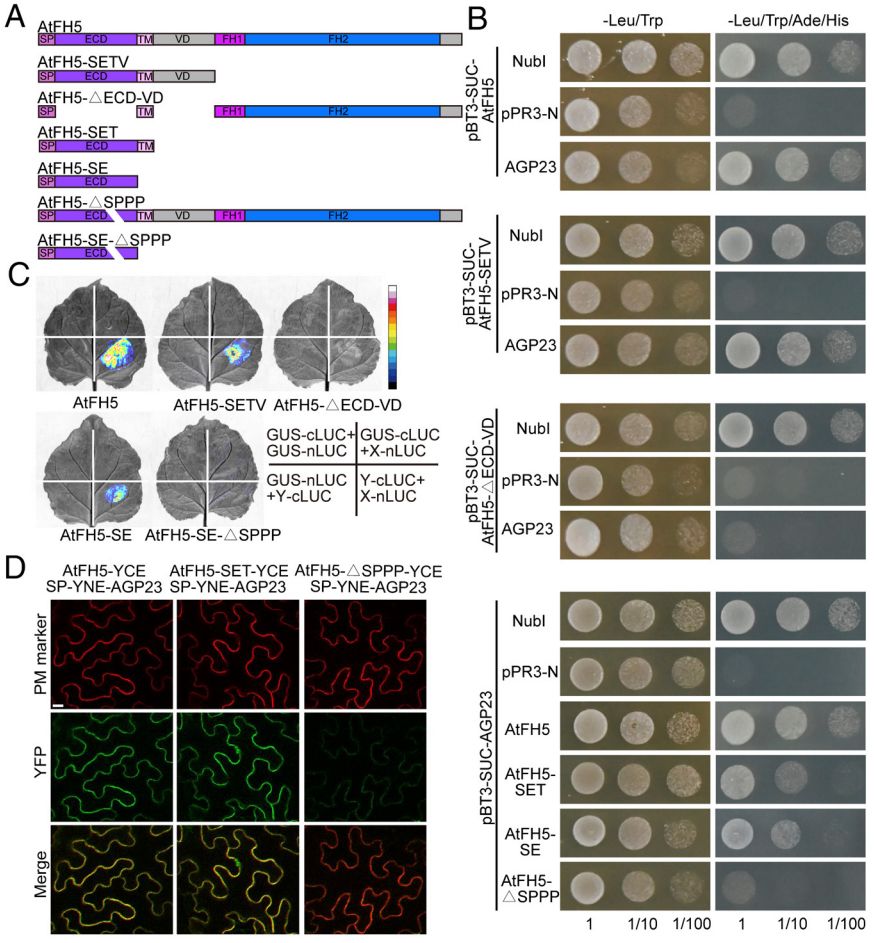


**Fig. 1.** The N-terminal of AtFH5 interacts with an arabinogalactan protein AGP23. (*A*) Full-length and different types of truncated AtFH5. SP, signal peptide; ECD, extracellular domain; TM, transmembrane domain; VD, variable domain; FH1 and FH2, Formin Homology domains. AtFH5-SETV (SP+ECD+TM+VD); AtFH5-△ECD-VD (SP+TM+FH1+FH2); AtFH5-SET (SP+ECD+TM); AtFH5-SE (SP+ECD); AtFH5-△SPPP (full-length AtFH5 with the EXT motif deletion); AtFH5-SE-△SPPP (AtFH5-SE with the EXT motif deletion); (*B*) Y2H assays showing that AtFH5 interacts with AGP23 via its ECD and EXT motif. The protein+NubI pair is used as a positive control, and the protein+pPR3-N pair is used as a negative control. (*C*) Split-LCAs showing that the interaction between AGP23 and AtFH5 needs the ECD and EXT motif. The GUS-cLUC+GUS-nLUC, GUS-cLUC+X-nLUC, and GUS-nLUC+Y-cLUC pairs are used as negative controls. (*D*) Bimolecular fluorescence complementation assays showing that the interaction between AGP23 and AtFH5 is weakened due to the EXT motif deletion. PM marker indicates the PM in tobacco leaf cells.

(*SI Appendix*, Fig. S1*E*). To explore the interacting domain, we constructed a series of vectors expressing different truncated AtFH5, including AtFH5-SETV (SP+ECD+TM+VD), AtFH5-△ECD-VD (SP+TM+FH1+FH2), AtFH5-SET (SP+ECD+TM), AtFH5-SE (SP+ECD), AtFH5-△SPPP (full-length AtFH5 with the EXT motif deletion), and AtFH5-SE-△SPPP (AtFH5-SE with the EXT motif deletion) (Fig. 1*A*). The results from Y2H, LCA, and bimolecular fluorescence complementation assays showed that full-length AGP23 interacted with full-length AtFH5, AtFH5-SETV, AtFH5-SET, and AtFH5-SE, but not with AtFH5-△ECD-VD (Fig. 1 *B*–*D*). These assays also revealed that deletion of the EXT motif of AtFH5 weakened its interaction with AGP23 (Fig. 1 *B* and *D* and *SI Appendix*, Fig. S1 *F* and *G*). These data suggest that the interaction between AtFH5 and AGP23 requires the ECD and the EXT motif of AtFH5.

**The *agp23* and *atfh5-3* Mutants Displayed Similar Defects during Pollen Germination and Tube Growth.** Although it is known that AGPs participate in pollen tube growth (25, 26, 31), the function of AGP23 has not been illustrated before. To test whether AGP23 is important for pollen germination and tube growth, we ordered two transfer DNA (T-DNA) mutants with low levels of *AGP23* expression and named them *agp23-1* and *agp23-2*, respectively (*SI Appendix*, Fig. S2 *A* and *B*). We observed the phenotypes of both mutants and compared them with *atfh5-3*, a reported mutant allele of *AtFH5* (12). Alexander staining showed that the pollen viability of these mutants was normal (*SI Appendix*, Fig. S2*C*). However, mutation of *AGP23* led to severe defects in pollen germination and pollen tube growth similar to *atfh5-3* (Fig. 2 *A*–*E*). The germination rate and pollen tube growth rate were significantly reduced in *agp23-1* and *agp23-2* compared with wild type, but showed no significant difference with *atfh5-3* (Fig. 2 *B* and *E*). Besides, the pollen tubes of these three mutants were more meandering than wild type with many turns (Fig. 2*A*, arrows, Fig. 2*C*). When pollens of *atfh5-3*, *agp23-1,* and *agp23-2* were germinated in WT stigma, some pollen tubes can still grow into embryo sacs (Fig. 2*F*), indicating that their response to the signals of guidance was not disrupted. To examine whether AtFH5 and AGP23 work in the same pathway, we applied β-Yariv, an inhibitor of AGPs (20), to WT, *atfh5-3*, and *agp23-2* pollens. Yariv treatment significantly decreased pollen germination rate in wild type, but did not further reduce pollen germination rate in these mutants (Fig. 2 *G* and *H*). The similar phenotype of *agp23* and *atfh5* mutants suggests that AGP23 may cooperate with AtFH5 to participate in the pollen germination and tube growth process.

**AGP23 Is Transported by AtFH5-Labeled Secretory Vesicles in Pollen.** The AGP23 deduced peptide contains only 61 amino acids with a SP at the N-terminal, *O*-glycosylation sites (*O*-GS) in the middle, and a glycosylphosphatidylinositol-anchor signal (GPI-AS) at the C-terminal (Fig. 3*A*). The biosynthesis of AGPs in the endoplasmic reticulum comprises the removal of SP and GPI-AS, the hydroxylation of proline residues, and the adding of a GPI anchor (20, 23). AGPs are then transferred to the Golgi apparatus for glycosylation and are finally transported by secretory vesicles to cell wall (20, 23, 24). To examine the subcellular localization of AGP23 and avoid the loss of fluorescent protein during AGP processing (35), we constructed a *pAGP23:SP-mTurquoise-AGP23* vector expressing an AGP23 fusion protein within which mTurquoise was located between the SP and the *O*-GS (Fig. 3*B*). The construct was driven by its native promoter and expressed in the *agp23-1* mutant background. The phenotype of *agp23-1* was fully rescued (*SI Appendix*, Fig. S3 *A* and *B*), suggesting that the mTurquoise-AGP23 line is functional. This line was further crossed with a reported line expressing AtFH5-mCherry (12).

Consistent with the previous report, AtFH5-mCherry-labeled vesicles gathered and underwent a rotational movement in germinating pollen grains (12) (Fig. 3 *C*–*E*). Most of mTurquoise-AGP23 co-localized with AtFH5-mCherry despite some weak signals out of the AtFH5-mCherry's cluster in pollen grains (Fig. 3*C*). Time-lapse imaging showed that mTurquoise-AGP23 conducted a synchronous rotational motion with AtFH5-mCherry (Fig. 3 *C*–*E* and Movie S1). Then, AtFH5-mCherry gathered at the prospective germination site and transferred to the cell surface of this region (Fig. 3 *C* and *F*, 150 to 360 s, white arrows, and Movie S1). Accompanied with AtFH5-mCherry's translocation to PM, mTurquoise-AGP23 also gathered at the germination site (Fig. 3 *C* and *F*, 150 to 360 s, white arrows, and Movie S1). We observed that the association with PM at the germination site of AtFH5 -mCherry and mTurquoise-AGP23 was not stable but rather weakened and recurred at the same site (Fig. 3 *C* and *F*, 150 to 360 s, 570 to 870 s, 960 to 1,320 s, arrows, and Movie S1). The 3D reconstruction analysis with a view facing the germination site and the co-localization analysis at this region revealed that mTurquoise-AGP23 and AtFH5-mCherry were co-localized at the germination site (Fig. 3*C*, 1,320 s, Fig. 3 *G* and *H*), despite that mTurquoise-AGP23 localized a little more external than AtFH5-mCherry at this region (Fig. 3*C*, 1,320 s, yellow box). To further investigate the relationship between AGP23 and AtFH5, we introduced the mTurquoise-AGP23 line into the *atfh5-3* mutant background and found that the aggregation and the rotational movement of mTurquoise-AGP23 were completely abolished in *atfh5-3* (Fig. 3 *I* and *J* and Movie S2). We either did not observe the location of mTurquoise-AGP23 at the germination site in *atfh5-3* (Fig. 3 *K* and *L* and Movie S2). These observations suggest that the dynamic localization of AGP23 in pollen grains is dependent on AtFH5.

To detect the spatiotemporal interaction between AtFH5 and AGP23 during pollen tube growth, we observed the signal in growing pollen tubes and found that mTurquoise-AGP23 and AtFH5-mCherry were accumulated and co-localized at the apical dome of pollen tube (Fig. 3 *M*–*O* and Movie S3). Both AtFH5-mCherry and mTurquoise-AGP23 showed PM localizations at apical and subapical regions, despite that the signal of AtFH5-mCherry was more evident (Fig. 3 *M* and *O*). Besides, mTurquoise-AGP23 displayed some weak signals in the pollen tube shank out of AtFH5-mCherry's cluster (Fig. 3*M*). To test whether AGP23 or AtFH5 is associated with cell wall, we performed plasmolysis assays and stained cell wall with propidium iodide (PI). After plasmolysis, we observed that both fluorescent protein-fused AGP23 and AtFH5 showed cell wall and PM localization at pollen tube tips (*SI Appendix*, Fig. S3 *C*–*F*, arrows). Besides, the plasmolysis treatment revealed that mTurquoise-AGP23 and AtFH5-mCherry were clearly co-localized at PM and cell wall of tip regions (Fig. 3 *P* and *Q*, arrows). However, the cell wall-associated signal of mTurquoise-AGP23 was disrupted in *atfh5-3* (Fig. 3 *R* and *S*, arrows). In contrast, the signal aggregation of another pollen wall protein, leucine-rich repeat extension 10 (LRX10) (36–38), at the germination site, appeared asynchronously with AtFH5-mCherry and was not affected while *AtFH5* mutation (*SI Appendix*, Fig. S3 *G*–*I*). These data suggest that AtFH5 determines the dynamic movement of AGP23 in pollen grains and its translocation to PM and cell wall at pollen tube tips.

To further test this conclusion, we also generated a *pLat52:SP-mCherry-AGP23* transgenic line, expressing mCherry-AGP23 driven by the *Lat52* promoter, in the Col-0 background and crossed it with *atfh5-3*. Consistently, mCherry-AGP23 was always dispersed, and showed neither rotation in pollen grains nor aggregation at the germination site in *atfh5-3* (*SI Appendix*, Fig. S3 *J*–*L* and Movie S4). Mutation of *AtFH5* also led to no cell wall-associated

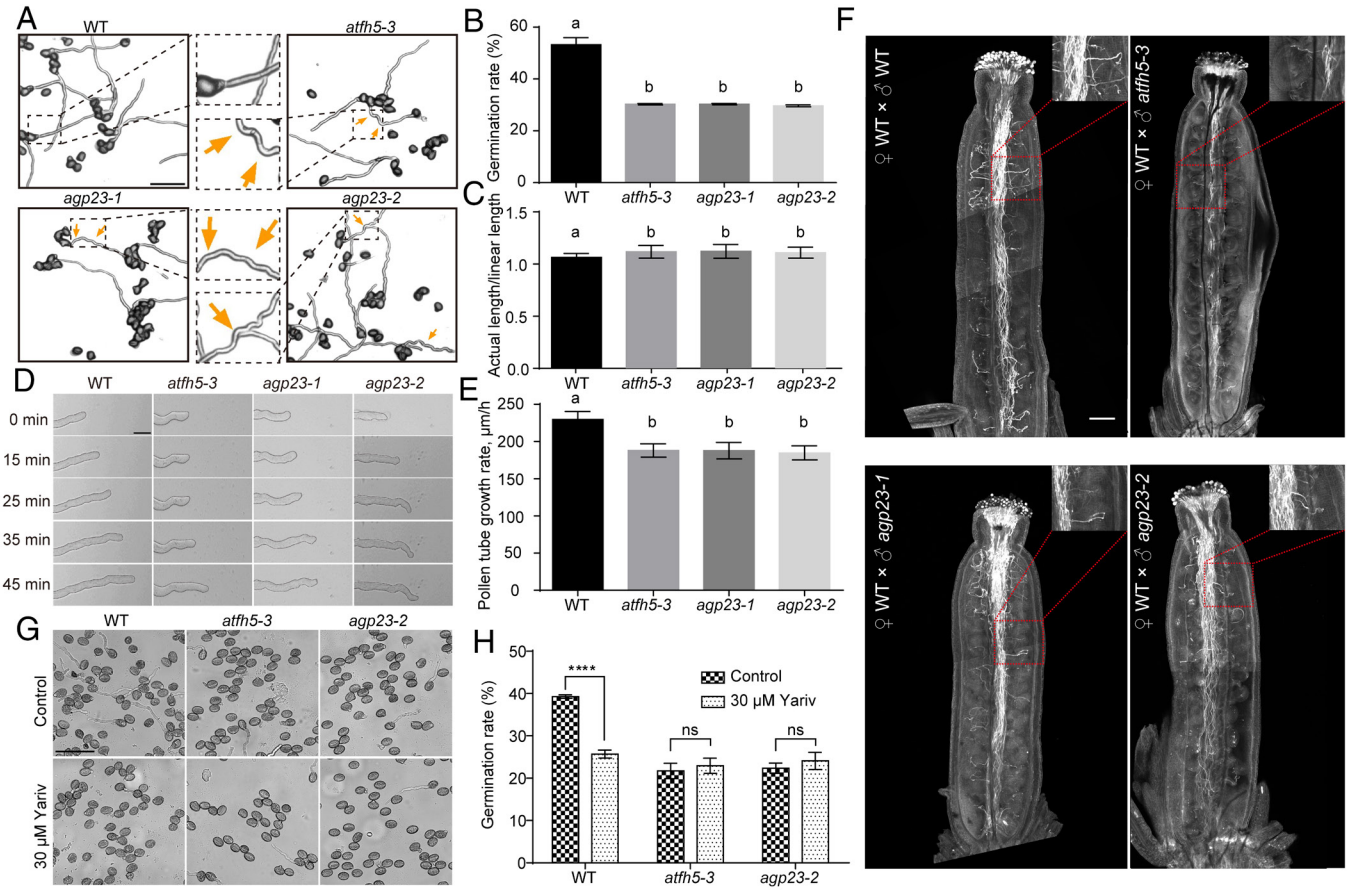


**Fig. 2.** The *agp23* and *atfh5-3* mutants displayed similar defects during pollen germination and tube growth. (*A*) Observation of pollen germination in wild type, *atfh5-3*, *agp23-1*, and *agp23-2*. Arrows indicate the turns of pollen tubes. Bar, 100 μm. (*B*) Pollen germination rate in wild type and mutants. (*C*) The curvature degree of pollen tubes represented by the ratio between actual length and linear length of pollen tubes. (*D*) Observation of pollen tube growth in wild type, *atfh5-3*, *agp23-1*, and *agp23-2*. Bar, 20 μm. (*E*) Pollen tube growth rate in wild type and mutants. Values in *B*, *C*, and *E* are means ± SD and the lowercases indicate $P < 0.05$, one-way ANOVA. (*F*) Semi-in vivo ovule targeting assay showing that pollen tubes from *atfh5-3*, *agp23-1*, and *agp23-2* are able to grow into WT embryo sacs. Bar, 200 μm. (*G*) Observation of pollen germination in the wild type, *atfh5-3*, and *agp23-2* after Yariv treatment. Bar, 20 μm. (*H*) Pollen germination rate with or without Yariv treatment. Values are mean±SD; ****$P < 0.0001$; ns, not significant; two-sided Student's *t* test.

signal of mCherry-AGP23 at pollen tube tips after plasmolysis (*SI Appendix*, Fig. S3 *M* and *N*, arrows). Combining these results with the interaction between AGP23 and AtFH5, the similarity of the phenotypes of their mutants, and their dynamic localization, we propose that AGP23 may be the cargo that is recruited and sorted by AtFH5, and transported by AtFH5-labeled secretory vesicles to the PM-cell wall destination during pollen germination and tube growth.

**The ECD and the EXT Motif of AtFH5 Contribute to AGP23 Transport.** As the normal interaction of AGP23 and AtFH5 requires the ECD and the EXT motif of AtFH5, we infer that the recruitment of AGP23 to AtFH5-labeled secretory vesicles may be mediated by this domain. To explore this assumption, we generated the *pAtFH5:gAtFH5-green fluorescent protein (GFP)*, *pAtFH5:gAtFH5-△ECD-GFP*, and *pAtFH5:gAtFH5-△SPPP-GFP* lines in the *atfh5-3* background (Fig. 4*A* and *SI Appendix*, Fig. S4*A*). The *pAtFH5:gAtFH5-GFP* line rescued the phenotype of *atfh5-3* to the WT level, but the *pAtFH5:gAtFH5-△ECD-GFP* and *pAtFH5:gAtFH5-△SPPP-GFP* lines failed to fully rescue the phenotype (Fig. 4 *B–F* and *SI Appendix*, Fig. S4 *B* and *C*). Pollen germination rate of the *pAtFH5:gAtFH5-△ECD-GFP* line was higher than that of the *atfh5-3* mutant but was significantly reduced compared with wild type, whereas pollen germination of the *pAtFH5:gAtFH5-△SPPP-GFP* line was not affected (Fig. 4 *B* and *C*). Besides, both lines showed decreased pollen tube growth rate and the meandering growth phenotype that similar to *atfh5-3* (Fig. 4 *D–F* and Movie S5). The failure in phenotype recovery suggests that the interacting sites of AtFH5 with AGP23 are essential for pollen germination and tube growth.

To further explore the function of the ECD and EXT motif of AtFH5, we crossed the *pAtFH5:gAtFH5-△ECD-GFP* or *pAtFH5:gAtFH5-△SPPP-GFP* line with the *pLat52:SP-mCherry-AGP23* line. AtFH5-GFP displayed a normal dynamic localization similar to AtFH5-mCherry (*SI Appendix*, Fig. S4 *D–I*). However, time-lapse imaging showed that deletion of the ECD of AtFH5 disrupted the aggregation and rotational movement of both AtFH5 and AGP23 in pollen grains (Fig. 4 *G* and *H* and Movie S6), as well as their gathering at the germination site (Fig. 4*G*, white band, Fig. 4*I* and Movie S6). During pollen tube growth, the deletion of ECD destroyed the membrane localization of AtFH5 and AGP23 (*SI Appendix*, Fig. S4 *J* and *K* and Movie S7), and their cell wall association after plasmolysis (Fig. 4 *J* and *K*, arrows). In line with this, we observed that the transgenic line fused expressing only the N-terminal (SP+ECD+TM) of AtFH5 or AtFH3, another Class I formin with distinct membrane-associated localization in pollen tubes (16, 19, 39), was able to display signal peaks at PMs of the subapical or shank region (*SI Appendix*, Fig. S4 *L–Q*). This result further supports that the ECD of Class I formins determines their membrane localization. In contrast with the ECD deletion, the EXT motif deletion of AtFH5 resulted in a weaker effect. AtFH5-△SPPP-GFP and mCherry-AGP23 displayed nearly

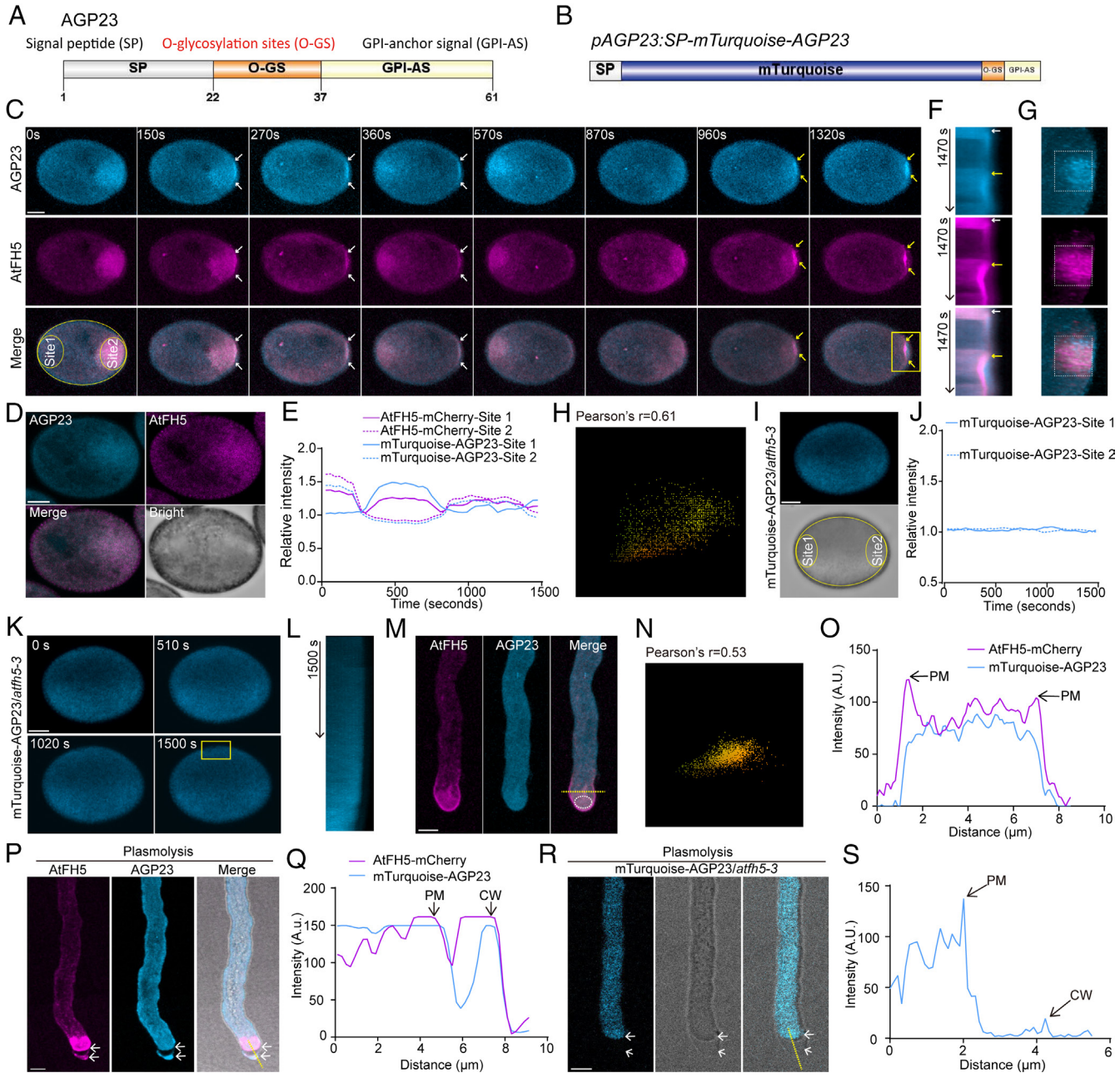


**Fig. 3.** AtFH5 recruits AGP23 to secretory vesicles, the germination site, and pollen tube tip. (*A*) The domain analysis of AGP23. SP, signal peptide; *O*-GS, *O*-glycosylation sites; GPI-AS, glycosylphosphatidylinositol-anchor signal. (*B*) The *pAGP23:SP-mTurquoise-AGP23* vector expressing an AGP23 fusion protein within which mTurquoise is located between SP and O-GS. (*C*) Representative time-lapse images of AtFH5-mCherry and mTurquoise-AGP23 during pollen germination. The white and yellow arrows indicate the prospective germination site during the first and the second time of association with the PM of AtFH5-mCherry and mTurquoise-AGP23, respectively. Bar, 5 μm. (*D*) A representative image showing the bright field image of a pollen grain. Bar, 5 μm. (*E*) Relative fluorescent intensity of AtFH5-mCherry and mTurquoise-AGP23 at site1 and site2 in *C*. (*F*) Kymograph analysis of AtFH5-mCherry and mTurquoise-AGP23 at the germination site indicated by the yellow box in *C*. The white and yellow arrows indicate the time point when the first and the second time of association with the PM of AtFH5-mCherry and mTurquoise-AGP23, respectively. (*G*) A 3D reconstruction analysis of the image of 1,320 s in *C* with a view facing the germination site. (*H*) Co-localization analysis of mTurquoise-AGP23 and AtFH5-mCherry at the germination site. The analyzed region was indicated with white boxes in *G*. (*I*) A representative image of mTurquoise-AGP23 in an *atfh5* pollen grain showing the analyzed region of site1 and site2. Bar, 5 μm. (*J*) Relative fluorescent intensity of mTurquoise-AGP23 in *atfh5-3* at site1 and site2 in *I*. (*K*) Representative time-lapse images of mTurquoise-AGP23 in *atfh5-3* during pollen germination. Bar, 5 μm. (*L*) Kymograph analysis of mTurquoise-AGP23 in *atfh5-3* at the germination site indicated by the yellow box in *K*. (*M*) A representative image showing AtFH5-mCherry and mTurquoise-AGP23 in a growing pollen tube. Bar, 5 μm. (*N*) Co-localization analysis of mTurquoise-AGP23 and AtFH5-mCherry at pollen tube tip indicated with a white oval in *M*. (*O*) Fluorescence intensity of AtFH5-mCherry and mTurquoise-AGP23 along the yellow line in *M*. The arrows indicate the PM. (*P*) Observation of AtFH5-mCherry and mTurquoise-AGP23 of a growing pollen tube after plasmolysis. Bar, 5 μm. (*Q*) Fluorescence intensity of AtFH5-mCherry and mTurquoise-AGP23 along the yellow line in *P*. The arrows indicate the PM and cell wall (CW), respectively. (*R*) Observation of mTurquoise-AGP23 in *atfh5-3* of a growing pollen tube after plasmolysis. Bar, 5 μm. (*S*) Fluorescence intensity of mTurquoise-AGP23 along the yellow line in *R*. The arrows indicate the PM and CW, respectively.

normal rotation during pollen germination (Fig. 4 *L* and *M* and Movie S8). Then, AtFH5-△SPPP-GFP was able to translocate to PM, whereas mCherry-AGP23 showed almost no signal at the germination site (Fig. 4*L*, white band, Fig. 4*N* and Movie S8). Similar to the phenotype in pollen grains, the deletion of EXT motif destroyed the membrane and cell wall localization of AGP23, but has little impact on the localization of AtFH5 (Fig. 4 *O* and *P*, arrows, *SI Appendix*, Fig. S4 *R* and *S*, and Movie S9). These data

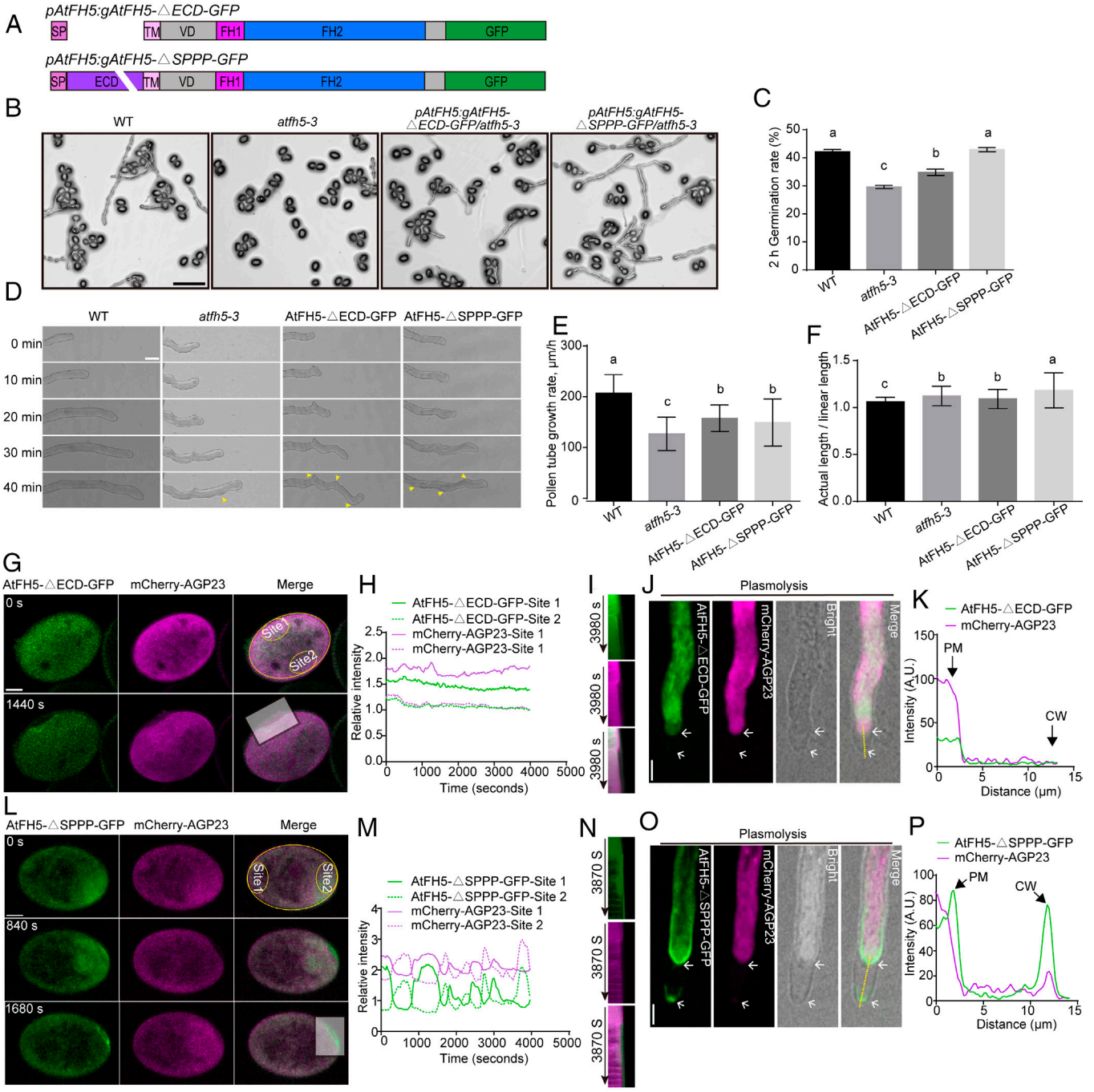


**Fig. 4.** The dynamic localization of AGP23 relies on the ECD and the EXT motif of AtFH5. (*A*) The *pAtFH5:gAtFH5-△ECD-GFP* vector expressing a truncated AtFH5 with the ECD deletion and fused with GFP; The *pAtFH5:gAtFH5-△SPPP-GFP* vector expressing a truncated AtFH5 with the EXT motif deletion and fused with GFP. (*B*) Observation of pollen germination in the wild type, *atfh5-3*, the *pAtFH5:gAtFH5-△ECD-GFP/atfh5-3* line, and the *pAtFH5:gAtFH5-△SPPP-GFP/atfh5-3* line. Bar, 200 μm. (*C*) Pollen germination rate in wild type, *atfh5-3*, the *pAtFH5:gAtFH5-△ECD-GFP/atfh5-3* line, and the *pAtFH5:gAtFH5-△SPPP-GFP/atfh5-3* line. (*D*) Observation of pollen tube growth in the wild type, *atfh5-3*, the *pAtFH5:gAtFH5-△ECD-GFP/atfh5-3* line, and the *pAtFH5:gAtFH5-△SPPP-GFP/atfh5-3* line. Bar, 20 μm. The arrow heads indicate the turns of pollen tubes. (*E*) The growth rate of pollen tubes in the wild type, *atfh5-3*, the *pAtFH5:gAtFH5-△ECD-GFP/atfh5-3* line, and the *pAtFH5:gAtFH5-△SPPP-GFP/atfh5-3* line. (*F*) The curvature degree of pollen tubes in the wild type, *atfh5-3*, the *pAtFH5:gAtFH5-△ECD-GFP/atfh5-3* line, and the *pAtFH5:gAtFH5-△SPPP-GFP/atfh5-3* line. Values in *C*, *E*, and *F* are means ± SD and the lowercases indicate $P < 0.05$, one-way ANOVA. (*G*) Representative time-lapse images of AtFH5-△ECD-GFP and mCherry-AGP23 during pollen germination. Bar, 5 μm. (*H*) Relative fluorescent intensity of AtFH5-△ECD-GFP and mCherry-AGP23 at site1 and site2 in *G*. (*I*) Kymograph analysis of AtFH5-△ECD-GFP and mCherry-AGP23 at the germination site indicated by the white band in *G*. (*J*) Observation of AtFH5-△ECD-GFP and mCherry-AGP23 of a growing pollen tube after plasmolysis. Bar, 5 μm. (*K*) Fluorescence intensity of AtFH5-△ECD-GFP and mCherry-AGP23 along the yellow line in *J*. The arrows indicate the PM and CW, respectively. (*L*) Representative time-lapse images of AtFH5-△SPPP-GFP and mCherry-AGP23 during pollen germination. Bar, 5 μm. (*M*) Relative fluorescent intensity of AtFH5-△SPPP-GFP and mCherry-AGP23 at site1 and site2 in *L*. (*N*) Kymograph analysis of AtFH5-△SPPP-GFP and mCherry-AGP23 at the germination site indicated by the white band in *L*. (*O*) Observation of AtFH5-△SPPP-GFP and mCherry-AGP23 of a growing pollen tube after plasmolysis. Bar, 5 μm. (*P*) Fluorescence intensity of AtFH5-△SPPP-GFP and mCherry-AGP23 along the yellow line in *O*. The arrows indicate the PM and CW, respectively.

suggest that the ECD and EXT motif of AtFH5 are required for the successful delivery of AGP23 from secretory vesicles to cell wall and deposition during pollen germination and tube growth.

**Loss of AtFH5 and AGP23 Affects the Cell Wall Composition.** AGPs are key cell wall components controlling tip plasticity during pollen tube growth (25, 40, 41). To test whether

mutation in *AGP23* and *AtFH5* alters cell wall composition, we carried on immunostaining assays to detect the proportion of some cell wall components. We also constructed the *atfh5-3 agp23-2* double mutant to dissect the genetic relationship between *AtFH5* and *AGP23*. The signal of LM2, an antibody probes for AGPs (20), was accumulated at WT pollen tube tips, but was significantly reduced in *atfh5-3*, *agp23-2*, and *atfh5-3 agp23-2* (Fig. 5 *A* and *B*). This further supports that normal level of AGPs at the cell wall of pollen tube tips requires the function of AtFH5. The signal of the JIM7 antibody, labeling highly methylesterified homogalacturonan (HG), was significantly increased at the apical region in *atfh5-3*, *agp23-2*, and *atfh5-3 agp23-2* compared with wild type (Fig. 5 *C* and *D*), whereas the apical signal of the JIM5 antibody (labeling low methylesterified HG) was slightly reduced in *atfh5-3*, *agp23-2*, and *atfh5-3 agp23-2* (Fig. 5 *E* and *F*). These data indicate that more highly methylesterified pectin and fewer low methylesterified pectin were deposited at the apex of pollen tubes, which may alter the mechanical properties of cell wall and the apical stiffness (25, 42–44). We also examined the level of callose by aniline blue staining. We detected that callose mainly label the shank region to the base of pollen tube and its contents in *atfh5-3*, *agp23-2*, and *atfh5-3 agp23-2* were significantly lower than that in the wild type (Fig. 5 *G* and *H*). Together, these results suggest that loss of AtFH5 and AGP23 affects the proportion of major cell wall components, and this may be the reason for reduced growth rate and the winding growth phenotype of pollen tubes.

## Discussion

AtFH5 is a multifunctional protein involved in many aspects of cytoskeletal organization and membrane trafficking. The distinct biochemical activities of AtFH5's different domains, as well as its dynamic localization from secretory vesicles to the cell wall-PM-cytoskeleton continuum, confer the protein versatile functions during pollen germination and pollen tube growth. AtFH5 is well known as a cytoskeletal regulator relying on its C-terminal FH1 and FH2 domains, which can effectively nucleate actin polymerization from actin and profilin-actin pools in vivo (45). Cell biological evidence also shows that AtFH5 plays an essential role in promoting actin polymerization and establishing actin filament-based structures both in pollen grains and tubes (12, 15). However, new functions of AtFH5 remain to be discovered, especially for the biological significance of its vesicle association and cell wall interaction via the N-terminal ECD.

In this study, we uncovered a role of AtFH5 in directing the sorting and deposition of cell wall components via vesicle trafficking during pollen germination and tube growth (Fig. 5 *I*–*K*). During pollen germination, AGP23 is recruited into AtFH5-labeled secretory vesicles through the interaction with the N-terminal ECD of AtFH5 (Fig. 5*I*). Thus, AGP23 is able to rotate along with AtFH5-labeled vesicles in pollen grains driven by actin polymerization mediated by the FH1 and FH2 domains of AtFH5 (Fig. 5*J*). Then, AtFH5-labeled vesicles carry AGP23 to the germination site and initiate the translocation of AtFH5 and AGP23 to PM and cell wall (Fig. 5 *J* and *K*). Deletion of the ECD of AtFH5 interrupts the rotation of vesicles and the localization of AtFH5 and AGP23 at the germination site, leading to severe defects in pollen germination. Deletion of the EXT motif has minor effect on vesicle movement, but affects AGP23's localization at the germination site, suggesting that the proper deposition of AGP23 at cell wall requires the EXT motif of AtFH5. During pollen tube growth, AGP23 also co-localizes with AtFH5-labeled vesicles at the apical region of tubes, and show evident association with PM and cell wall at tube tips. Deletions of the ECD and EXT motif of AtFH5 alter cell wall composition and the tip growth of pollen tubes (Fig. 5 *J* and *K*). Based on these observations, we propose that AtFH5 functions like an active "conductor" and "helmsman," but not a passive "passenger," to precisely sort the cargos in AtFH5-labeled vesicles and steer the transport of itself and others to the PM-cell wall destination during pollen germination and tube growth. This study provides insights into intracellular sorting and trafficking of cell wall materials from a cytoskeletal perspective, which enhances our understanding of the crosstalk between the cytoskeleton system and cell wall in plant cells.

Bioinformatics analysis shows that the ECD of plant Class I formins contain a conserved cell wall-related EXT motif (Ser-$Hyp_{3\text{-}5}$), and some emerging evidence suggests that formins' ECD is required for their cell wall anchoring and membrane localization (16–19), which is a common feature of plant Class I formins and is essential for the membrane-derived actin polymerization (46). Consistently, our results showed that the deletion of ECD of AtFH5 caused dispersed localizations of both AtFH5 and its interacting factor AGP23. Further, these data also indicate that the ECD of AtFH5 not only mediates the membrane anchorage of itself but also regulates the recruitment and trafficking of some cargos of AtFH5-labeled vesicles. In line with this, a recent finding showed that AtFH5-decorated vesicles carry the calcium-permeable channel CNGC18 to promote calcium oscillation and periodic exocytosis during pollen germination (13). Moreover, a recent review proposed an "active cargoes" theory of plant class I formins for their function in modulating the fate of endo- or exocytotic systems while being transported by them (47). Thus, as a key linker of the cytoskeleton system and the endomembrane system, AtFH5 is much more powerful than the conventional thought in pollen.

AGPs interact with cell wall components and PM proteins to regulate plant development and growth, yet the exact mechanisms remain elusive (41). Our genetic and cytological evidence suggests that AtFH5 and AGP23 work in the same pathway during regulating cell wall composition and pollen tube growth. The content of highly methylesterified HG was increased and the level of callose was reduced in *atfh5-3*, *agp23-2*, and the *atfh5-3 agp23-2* double mutant, indicating that cell wall composition was severely altered. It is known that AGPs serve as crosslinkers covalently connected with pectins or other cell wall elements; thus, changes in AGPs may determine the presence and distribution of other components (24, 25, 41). In support of our finding, knockout of hydroxyproline-*O*-galactosyltransferases required for AGP glycosylation caused multiple pollen development defects in *Arabidopsis*, and the *hpgt1, 2, 3* triple mutant also displayed a reduction in cellulose and an accumulation of pectin (48, 49). Our data provide a molecular link between the vesicle trafficking of AGPs and cell wall composition mediated by the ECD of AtFH5 during pollen germination and tube growth. However, there are some open questions that need further investigations as to the dynamic interplay between AtFH5 and AGP23. First, although most of AGP23 co-localized well with AtFH5, it showed some weak signals out of the AtFH5 cluster no matter in pollen grains or pollen tubes. These data imply that AtFH5-decorated vesicles may not be the only delivery route of AGP23. Besides, whether the function in cargo recruitment of AtFH5 is specific to AGP23 or can be applied to other cell wall components still unclear. In our screen of AtFH5 interactors, many other cell wall proteins were indeed identified but is pending further verification.

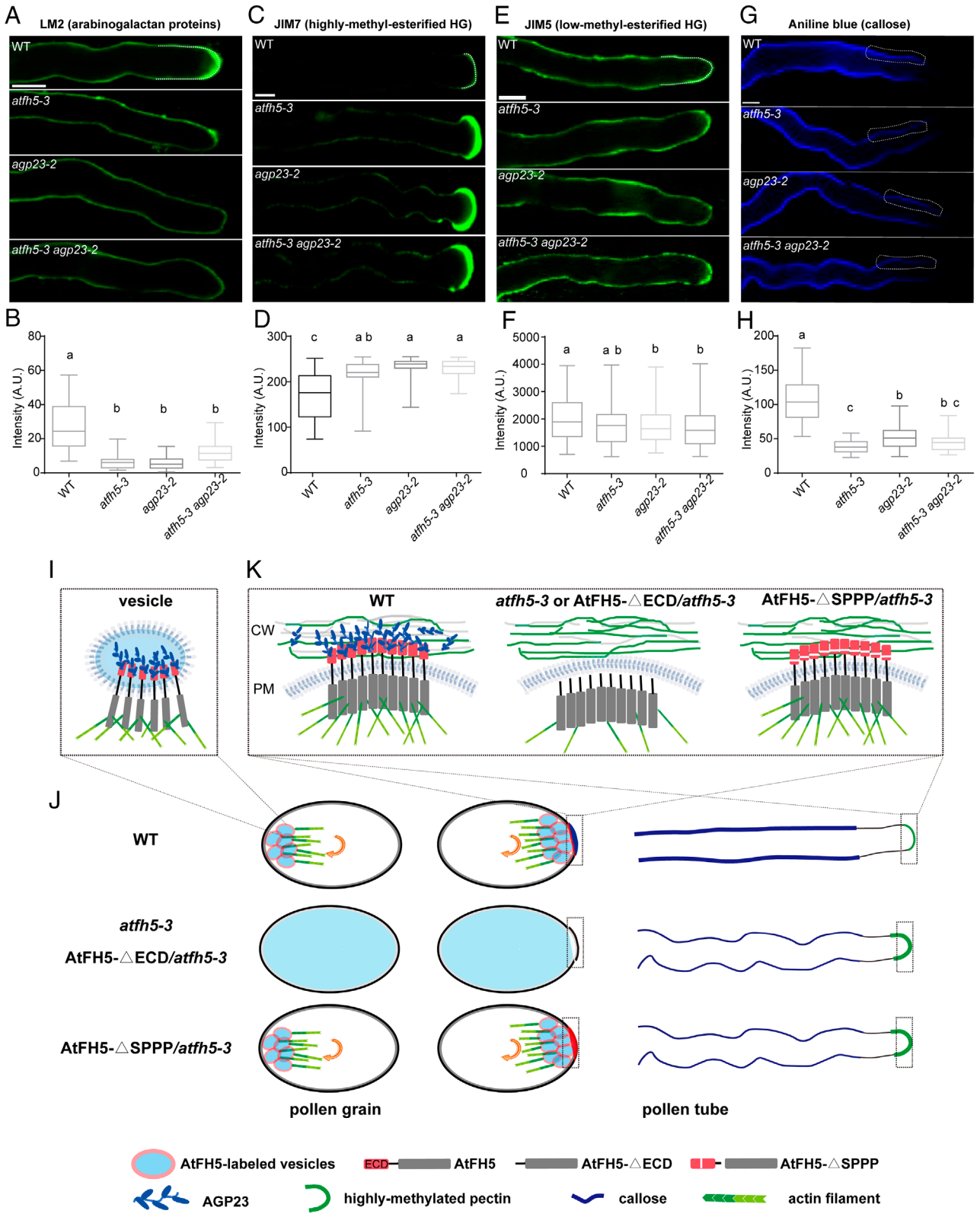


**Fig. 5.** AtFH5 and AGP23 work together to regulate cell wall composition and the proposed working model. (*A*) Immunolabeling of pollen tubes of wild type, *atfh5-3*, *agp23-2,* and the *atfh5-3 agp23-2* double mutant using the LM2 antibody. Bar, 5 μm. (*B*) Quantitative analysis of the relative fluorescence intensity of LM2. (*C*) Immunolabeling of pollen tubes of wild type, *atfh5-3*, *agp23-2,* and *atfh5-3 agp23-2* using the JIM7 antibody. Bar, 5 μm. (*D*) Quantitative analysis of the relative fluorescence intensity of JIM7. (*E*) Immunolabeling of pollen tubes of wild type, *atfh5-3*, *agp23-2,* and *atfh5-3 agp23-2* using the JIM5 antibody. Bar, 5 μm. (*F*) Quantitative analysis of the relative fluorescence intensity of JIM5. (*G*) Aniline blue staining of pollen tubes in wild type, *atfh5-3*, *agp23-2,* and *atfh5-3 agp23-2*. Bar, 5 μm. The white dotted lines indicate the analysis region of the fluorescence intensity in *A*, *C*, *E*, and *G*. (*H*) Quantitative analysis of the relative fluorescence intensity of Aniline blue. Values in *B*, *D*, *F*, and *H* are means ± SD and the lowercases indicate $P < 0.05$, one-way ANOVA. (*I*–*K*) The proposed working model for AtFH5-mediated recruitment, transport, and deposition of AGP23 during pollen germination and tube growth. First, AtFH5 localizes at secretory vesicles and promotes actin polymerization to drive vesicle trafficking during pollen germination; meanwhile, AtFH5 recruits cell wall components, like AGP23, to these vesicles via its ECD and the EXT motif (*I* and *J*). Second, the AtFH5-labeled vesicles carry AGPs to the cell surface destination and determine their disposition at cell wall of growing tips (*J* and *K*). Third, loss of *AtFH5*, ECD, or the EXT motif disrupts the transport and deposition of AGP23, and finally alters cell wall composition and the tip growth of pollen tubes (*J* and *K*).

## Materials and Methods

**Plant Materials.** The background of WT *Arabidopsis thaliana* is Col-0. The T-DNA insertion mutants, *agp23-1* (WiscDsLox2C2) and *agp23-2* (WiscDsLox461-464G12), were obtained from the *Arabidopsis* Biological Resource Center. The *atfh5-3* mutant (salk_152090) and the *pAtFH5:gAtFH5-mCherry/atfh5-3* transgenic line were previously reported (12). The *pLRX10:gLRX10-GFP/lrx8lxr9lrx10* line was a generous gift of Prof. Yi Guo from Hebei Normal University (36). All *Arabidopsis* seeds were sterilized and vernalized at 4 °C for 2 d, transferred to a greenhouse for 6 to 7 d (22 °C, 16 h light/8 h dark cycle), and then the seedlings were moved to soil for further culture.

**Vector Construction and Plant Transformation.** To detect the subcellular localization of AGP23 and obtain complementation, the *AGP23* (*AT3G57690*) putative promoter, including the 2 kb fragment upstream of the start codon, the SP, and the remaining sequence, were separately amplified from wild type genomic DNA. The mTurquoise-coding sequence was cloned from the *pCambia1300-mTurquoise* vector. All the amplified segments were inserted into an empty *pCambia1305* vector to construct the *pAGP23:SP-mTurquoise-AGP23* plasmid using the ClonExpress Ultra One Step Cloning Kit V2 (Vazyme). Then, this plasmid was transformed into the *atagp23-1* background via *Agrobacterium tumefaciens* (strain GV3101)-mediated floral dip method. The construction of *pLat52:SP-mCherry-AGP23* was similar to *pAGP23:SP-mTurquoise-AGP23* with the promoter replaced by *Lat52* and the fluorescent protein replaced by mCherry. This vector was transformed into the Col-0 background. To generate the *pAtFH5:gAtFH5-GFP, pAtFH5:gAtFH5-*$^{\triangle}$*ECD-GFP*, and *pAtFH5:gAtFH5-*$^{\triangle}$*SPPP-GFP* vectors, the *AtFH5* putative promoter (approximately 2 kb), full-length genomic sequence or truncated genome regions of *AtFH5*, and the GFP-coding sequence, were amplified and inserted into the *pCambia1305* vector. Then, these recombinant vectors were separately transformed into the *atfh5-3* mutant plants. To generate the *pLat52:AtFH3-SP-ECD-TM-GFP* and *pLat52:AtFH5-SP-ECD-TM-GFP* construct, the coding sequence of the N-terminal of *AtFH3* (*AT4G15200*) or *AtFH5* (*AT5G54650*) was separately amplified using *Arabidopsis* cDNA) as template, and inserted into the KpnI/BamHI sites of the *pCambia1305-Lat52-GFP* vector using 2× Phanta Flash Master Mix (Vazyme). These vectors were transformed into the Col-0 background. All the primers are listed in *SI Appendix*, Table S2.

**Pollen Germination and Plasmolysis Analysis In Vitro.** Pollen grains were obtained from flowering plants (4 to 6 wk old) and were cultured at 28 °C on the pollen germination solid medium [1 mM $CaCl_2$, 1 mM Ca $(NO_3)_2$, 1 mM $MgSO_4$, 0.01% $H_3BO_3$, 18% sucrose, and 0.15% agar, pH 6.9 to 6.95] for germination. To observe pollen germination and tube growth, pollen grains were cultured on the pollen germination solid medium at 28 °C for 3 h. The pollen germination rate and the curvature degree of pollen tubes were analyzed using ImageJ. The curvature degree of pollen tubes was represented by the ratio between the actual length and the linear length of pollen tubes. For the pollen tube plasmolysis assay, the pollen germination liquid medium [1 mM $CaCl_2$, 1 mM Ca $(NO_3)_2$, 1 mM $MgSO_4$, 0.01% $H_3BO_3$, 18% sucrose, pH 6.9 to 6.95] containing 50% sucrose were added to pollen tubes after normal culturing for 2 to 3 h, and then were observed and photographed 5 min later.

**Time-Lapse Imaging.** Pollen grains were cultured for 30 min and then photographed under a spinning-disk confocal microscope (UltraView VoX, PerkinElmer, Beaconsfield, Buckinghamshire, UK) equipped with the Yokogawa Nipkow CSU-X1 spinning disk scanner, a Nikon TiE inverted microscope with a 633/1.4 objective, and a Hamamatsu EMCCD 9100-13. The 445, 488, and 561 nm lasers were used for imaging. The time interval is 30 s, and the Z-axis interval is 0.5 μm in the shooting process.

**DUAL Membrane Y2H Assay.** The vectors used in the DUAL membrane Y2H assay were *pBT3-SUC* (bait vector) and *pPR3-N* (prey vector). Full-length AGP23 and different types of truncated AtFH5 sequences were amplified using primers listed in *SI Appendix*, Table S2 and separately cloned into the pBT3-SUC and pPR3-N vectors. The protein+NubI pair is used as a positive control, and the protein+pPR3-N pair is used as a negative control. Different vector pairs were co-transformed into the yeast strain NMY51 as described before (50). Positive clones growing on the selective medium -Trp/Leu indicates successful transformation, and positive clones growing on the selective medium -Leu/Trp/Ade/His indicates the interaction between two proteins.

**LCA.** The *pCambia1300-NLuc* and *pCambia1300-CLuc* vectors used in the luciferase complementation experiment were donated by Prof. Jianmin Zhou, the Institute of Genetics and Developmental Biology, Chinese Academy of Sciences (51). The coding sequences of the candidate genes were amplified using primers listed in *SI Appendix*, Table S2 and cloned into the *pCambia1300-NLuc* or *pCambia1300-CLuc* vector. The GUS-cLUC+GUS-nLUC, GUS-cLUC+protein-nLUC, and GUS-nLUC+protein-cLUC pairs are used as negative controls. The vector pairs were transformed into *Agrobacterium* (strain GV3101) and the cultured bacteria were suspended in the buffer (10 mM MgCl2, 10 mM 4-Morpholineethanesulfonic acid, pH 5.6) containing 100 mM acetosyringone to a final concentration of $OD_{600}$ = 1.0. Different *Agrobacterium* with different vector pairs were mixed in a ratio of 1:1. The suspension was infiltrated into 4-wk-old *N. tabacum* leaves. The plants were placed in dark for 18 h, and then transferred to a room under a 16 h/8 h light/dark cycle for 48 h. Detached leaves smeared with 1 mM luciferin, then kept in darkness for 7 to 10 min and were observed with a cooled CCD (FLI) imaging apparatus (Lumazone CA 1300B).

**Bimolecular Fluorescence Complementation Assay.** The vectors used in the bimolecular fluorescence complementation assay were *p35S:SPYCE (M)* and *p35S:SPYNE173* (52). The coding sequences of the candidate genes were amplified using primers listed in *SI Appendix*, Table S2 and cloned into *p35S:SPYCE (M)* or *p35S:SPYNE173*. The subsequent transformation of *Agrobacterium* and the transient transformation of *N. tabacum* leaves were the same as described in the LCA. The transformed leaves were observed under the FV300RS microscope (Olympus) using the 514 nm laser.

**Yariv Treatment.** Pollen grains of wild type, *atfh5-3,* and *agp23-2* were cultured in the pollen germination solid medium containing 30 μM Yariv reagents at 28 °C for 1.5 h. Pollen germination was observed by Axio Observer 7 microscope (ZEISS) and the pollen germination rate was calculated using ImageJ.

**Alexander Staining.** Mature pollen grains were dispersed on pollen germination solid medium and the Alexander stain Solution (Solarbio G3050) was added to cover all pollen grains on the medium. Then pollen viability was observed under a light microscope (Olympus IX83).

**Immunofluorescence Assay.** The immunofluorescence assay was conducted following the described procedures (53, 54). In brief, pollen tubes were grown on solid pollen germination medium for 3 h. Then, 4% (w/v) paraformaldehyde in pollen germination liquid medium was added to pollen grains for 30 min at room temperature. After three times of wash with 1× PBS, they were blocked with 1× phosphate buffered saline (PBS) containing 3% bovine serum albumin (BSA) at room temperature for 1 h. Samples were incubated at room temperature for 1 h (or at 4 °C overnight) in dark with the rat primary antibody (LM2, JIM7, or JIM5) in 1× PBS containing 3% BSA. LM2 and JIM7antibodies were diluted at a ratio of 1:100, JIM5 antibody was diluted at a ratio of 1:5. Samples were washed out with 1× PBS three times. The secondary antibody was Rabbit Anti-Rat IgM (HL)-Alexa Fluor 488 or Rabbit Anti-Rat IgA (HL)-Alexa Fluor 488. It was diluted at a ratio of 1:200 and added to pollen grains, followed by incubating them for 2 h at room temperature in the dark. After wash, the samples were observed and imaged under LSM 980 with Airyscan 2 (ZEISS) using 488 nm laser.

**Semi-In Vivo Ovule Targeting Assay.** Pollen grains were germinated in WT stigma for 24 h. Then, the pollinated stigmas were cut off and put into the fixing buffer (ethanol: acetic acid = 3:1) for 1.5 h. After removal of the fixing buffer, stigmas were washed with 70%, 50%, 30% ethanol and $ddH_2O$, respectively. These stigmas were softened by soaking in 8 M NaOH for 8 to 12 h, washed with $ddH_2O$ for three times, and then stained with 0.1% aniline blue for 3 h in dark. The stained stigmas were observed under LSM 980 with Airyscan 2 (ZEISS) using 405 nm laser.

**Aniline Blue Staining.** Pollen grains were cultured on pollen germination solid medium for 3 h, fixed using a fixative (4% [w/v] paraformaldehyde in pollen germination liquid medium), and then were washed three times with 100 mM phosphate buffer. The water-soluble aniline blue powder was used to prepare 0.1% aniline blue

staining liquid, which was directly added to the pollen tubes for 30 min. Then, these pollen tubes were observed using 405 nm laser under LSM 980 with Airyscan 2 (ZEISS).

**PI Staining.** Pollen tubes were grown on solid pollen germination medium for 2 h and then 20 μM PI in pollen germination liquid medium was added to stain pollen tubes for 5 min. Pollen tubes were observed under the FV300RS microscope (Olympus) using 405 nm laser.

**Statistical Analysis.** All microscope images obtained in the experiment were measured, statistically analyzed using ImageJ (Win64) and GraphPad Prism 6.01, and significance differences between multiple sets of data were analyzed using One-way ANOVA method.

**Data, Materials, and Software Availability.** All study data are included in the article and/or supporting information.

**ACKNOWLEDGMENTS.** We acknowledge Prof. Yi Guo, Hebei Normal University, for the share of the *pLRX10:gLRX10-GFP/lrx8lxr9lrx10* line. We acknowledge Dr. Xiaoyan Zhang, College of Life Sciences, Beijing Normal University, for the technical support. We acknowledge Dr. Pingzhou Du, Instrumentation and Service Center for Science and Technology, Beijing Normal University, Zhuhai, for the technical support. This work was supported by grants from the National Natural Science Foundation of China (92254303 and 32170335 to H. Ren) and the National Key Research and Development Program of China (2023YFD1201700 to F.Z.).

Author affiliations: [a]Department of Biology, Key Laboratory of Cell Proliferation and Regulation Biology of Ministry of Education, College of Life Science, Beijing Normal University, Beijing 100875, China; and [b]Center for Biological Science and Technology, Guangdong Zhuhai-Macao Biotechnology Joint Laboratory, Beijing Normal University, Zhuhai 519087, China

1. P. K. Hepler, C. M. Rounds, L. J. Winship, Control of cell wall extensibility during pollen tube growth. *Mol. Plant* **6**, 998–1017 (2013).
2. M. Cascallares *et al.*, A complex journey: Cell wall remodeling, interactions, and integrity during pollen tube growth. *Front. Plant Sci.* **11**, 599247 (2020).
3. G. J. Hao *et al.*, Vesicle trafficking in pollen tubes. *FEBS Lett.* **596**, 2231–2242 (2022).
4. Y. Fu, The cytoskeleton in the pollen tube. *Curr. Opin. Plant Biol.* **28**, 111–119 (2015).
5. H. Q. Ruan, J. Li, T. Wang, H. Y. Ren, Secretory vesicles targeted to plasma membrane during pollen germination and tube growth. *Front. Cell Dev. Biol.* **8**, 615447 (2021).
6. R. H. Zhang, Y. A. Xu, R. Yi, J. F. Shen, S. J. Huang, Actin cytoskeleton in the control of vesicle transport, cytoplasmic organization, and pollen tube tip growth. *Plant Physiol.* **193**, 9–25 (2023).
7. G. Cai, L. Parrotta, M. Cresti, Organelle trafficking, the cytoskeleton, and pollen tube growth. *J. Integr. Plant Biol.* **57**, 63–78 (2015).
8. F. W. Gu, E. Nielsen, Targeting and regulation of cell wall synthesis during tip growth in plants. *J. Integr. Plant Biol.* **55**, 835–846 (2013).
9. Y. Gu, C. G. Rasmussen, Cell biology of primary cell wall synthesis in plants. *Plant Cell* **34**, 103–128 (2022).
10. L. Liu *et al.*, Actomyosin and CSI1/POM2 cooperate to deliver cellulose synthase from Golgi to cortical microtubules in *Arabidopsis*. *Nat. Commun.* **14**, 7442 (2023).
11. P. A. C. van Gisbergen, M. Bezanilla, Plant formins: Membrane anchors for actin polymerization. *Trends Cell Biol.* **23**, 227–233 (2013).
12. C. Liu, Y. Zhang, H. Y. Ren, Actin polymerization mediated by AtFH5 directs the polarity establishment and vesicle trafficking for pollen germination in *Arabidopsis*. *Mol. Plant* **11**, 1389–1399 (2018).
13. H. Q. Ruan, T. Wang, H. Y. Ren, Y. Zhang, AtFH5-labeled secretory vesicles-dependent calcium oscillation drives exocytosis and stepwise bulge during pollen germination. *Cell Rep.* **42**, 113319 (2023).
14. C. Liu, Y. Zhang, H. Y. Ren, Profilin promotes formin-mediated actin filament assembly and vesicle transport during polarity formation in pollen. *Plant Cell* **33**, 1252–1267 (2021).
15. A. Y. Cheung, S. Niroomand, Y. J. Zou, H. M. Wu, A transmembrane formin nucleates subapical actin assembly and controls tip-focused growth in pollen tubes. *Proc. Natl. Acad. Sci. U.S.A.* **107**, 16390–16395 (2010).
16. Y. X. Lan, X. N. Liu, Y. Fu, S. J. Huang, Class I formins control membrane-originated actin polymerization at pollen tube tips. *PLoS Genet.* **14**, e1007789 (2018).
17. P. B. Liang *et al.*, Formin-mediated bridging of cell wall, plasma membrane, and cytoskeleton in symbiotic infections of *Medicago truncatula*. *Curr. Biol.* **31**, 2712–2719 (2021).
18. A. Martiniere, P. Gayral, C. Hawes, J. Runions, Building bridges: Formin1 of *Arabidopsis* forms a connection between the cell wall and the actin cytoskeleton. *Plant J.* **66**, 354–365 (2011).
19. C. M. Lara-Mondragón, A. Dorchak, C. A. MacAlister, *O*-glycosylation of the extracellular domain of pollen class I formins modulates their plasma membrane mobility. *J. Exp. Bot.* **73**, 3929–3945 (2022).
20. G. J. Seifert, K. Roberts, The biology of arabinogalactan proteins. *Annu. Rev. Plant Biol.* **58**, 137–161 (2007).
21. S. H. Su, T. Higashiyama, Arabinogalactan proteins and their sugar chains: Functions in plant reproduction, research methods, and biosynthesis. *Plant Reprod.* **31**, 67–75 (2018).
22. E. Nguema-Ona, M. Vicré-Gibouin, M. A. Cannesan, A. Driouich, Arabinogalactan proteins in root-microbe interactions. *Trends Plant Sci.* **18**, 445–454 (2013).
23. J. Silva, R. Ferraz, P. Dupree, A. M. Showalter, S. Coimbra, Three decades of advances in arabinogalactan-protein biosynthesis. *Front. Plant Sci.* **11**, 610377 (2020).
24. M. Ellis, J. Egelund, C. J. Schultz, A. Bacic, Arabinogalactan-proteins: Key regulators at the cell surface. *Plant Physiol.* **154**, 1012–1012 (2010).
25. D. T. A. Lamport, L. Tan, M. A. Held, M. J. Kieliszewski, Pollen tube growth and guidance: Occam's razor sharpened on a molecular arabinogalactan glycoprotein rosetta stone. *New Phytol.* **217**, 491–500 (2018).
26. E. Nguema-Ona, S. Coimbra, M. Vicré-Gibouin, J. C. Mollet, A. Driouich, Arabinogalactan proteins in root and pollen-tube cells: Distribution and functional aspects. *Ann. Bot.* **110**, 383–404 (2012).
27. A. M. Pereira, L. G. Pereira, S. Coimbra, Arabinogalactan proteins: Rising attention from plant biologists. *Plant Reprod.* **28**, 1–15 (2015).
28. A. Y. Cheung, H. Wang, H. M. Wu, A floral transmitting tissue-specific glycoprotein attracts pollen tubes and stimulates their growth. *Cell* **82**, 383–393 (1995).
29. H. M. Wu, H. Wang, A. Y. Cheung, A pollen-tube growth-stimulatory glycoprotein is deglycosylated by pollen tubes and displays a glycosylation gradient in the flower. *Cell* **82**, 395–403 (1995).
30. L. G. Pereira, S. Coimbra, H. Oliveira, L. Monteiro, M. Sottomayor, Expression of arabinogalactan protein genes in pollen tubes of *Arabidopsis thaliana*. *Planta* **223**, 374–380 (2006).
31. S. Coimbra *et al.*, Early germination of *Arabidopsis* pollen in a double null mutant for the arabinogalactan protein genes *AGP6* and *AGP11*. *Sex. Plant Reprod.* **23**, 199–205 (2010).
32. B. Levitin, D. Richter, I. Markovich, M. Zik, Arabinogalactan proteins 6 and 11 are required for stamen and pollen function in *Arabidopsis*. *Plant J.* **56**, 351–363 (2008).
33. M. Costa *et al.*, Expression-based and co-localization detection of arabinogalactan protein 6 and arabinogalactan protein 11 interactors in *Arabidopsis* pollen and pollen tubes. *BMC Plant Biol.* **13**, 7 (2013).
34. E. Marzol *et al.*, Filling the gaps to solve the extensin puzzle. *Mol. Plant* **11**, 645–658 (2018).
35. C. Borassi *et al.*, A cell surface arabinogalactan-peptide influences root hair cell fate. *New Phytol.* **227**, 732–743 (2020).
36. X. X. Wang *et al.*, Pollen-expressed leucine-rich repeat extensins are essential for pollen germination and growth. *Plant Physiol.* **176**, 1993–2006 (2018).
37. T. N. Fabrice *et al.*, LRX proteins play a crucial role in pollen grain and pollen tube cell wall development. *Plant Physiol.* **176**, 1981–1992 (2018).
38. M. A. Mecchia *et al.*, RALF4/19 peptides interact with LRX proteins to control pollen tube growth in *Arabidopsis*. *Science* **358**, 1600–1603 (2017).
39. J. R. Ye *et al.*, Formin 3 directs the formation of actin cables and polarized growth in pollen tubes. *Plant Cell* **21**, 3868–3884 (2009).
40. L. Tan *et al.*, An cell wall proteoglycan consists of pectin and arabinoxylan covalently linked to an arabinogalactan protein. *Plant Cell* **25**, 270–287 (2013).
41. S. Lin *et al.*, Arabinogalactan proteins: Focus on the role in cellulose synthesis and deposition during plant cell wall biogenesis. *Int. J. Mol. Sci.* **23**, 6578 (2022).
42. R. Zerzour, J. Kroeger, A. Geitmann, Polar growth in pollen tubes is associated with spatially confined dynamic changes in cell mechanical properties. *Dev. Biol.* **334**, 437–446 (2009).
43. A. J. Bidhendi, A. Geitmann, Relating the mechanics of the primary plant cell wall to morphogenesis. *J. Exp. Bot.* **67**, 449–461 (2016).
44. J. Du, C. T. Anderson, C. W. Xiao, Dynamics of pectic homogalacturonan in cellular morphogenesis and adhesion, wall integrity sensing and plant development. *Nat. Plants* **8**, 332–340 (2022).
45. M. Ingouff *et al.*, Plant formin AtFH5 is an evolutionarily conserved actin nucleator involved in cytokinesis. *Nat. Cell Biol.* **7**, U374–U380 (2005).
46. F. Cvrcková, Formins and membranes: Anchoring cortical actin to the cell wall and beyond. *Front. Plant Sci.* **4**, 436 (2013).
47. F. Cvrcková, R. Ghosh, H. Kocová, Transmembrane formins as active cargoes of membrane trafficking. *J. Exp. Bot.* **75**, 3668–3684 (2024), 10.1093/jxb/erae078.
48. D. Kaur, D. Moreira, S. Coimbra, A. M. Showalter, Hydroxyproline-galactosyltransferases synthesizing type II arabinogalactans are essential for male gametophytic development in *Arabidopsis*. *Front. Plant Sci.* **13**, 935413 (2022).
49. R. Okawa, Y. Hayashi, Y. Yamashita, Y. Matsubayashi, M. Ogawa-Ohnishi, Arabinogalactan protein polysaccharide chains are required for normal biogenesis of plasmodesmata. *Plant J.* **113**, 493–503 (2023).
50. G. H. Chen *et al.*, Identification and screening of host proteins interacting with ORFV-ORF047 protein. *Virol. J.* **18**, 27 (2021).
51. H. M. Chen *et al.*, Firefly luciferase complementation imaging assay for protein-protein interactions in plants. *Plant Physiol.* **146**, 368–376 (2008).
52. R. Waadt *et al.*, Multicolor bimolecular fluorescence complementation reveals simultaneous formation of alternative CBL/CIPK complexes. *Plant J.* **56**, 505–516 (2008).
53. H. X. Li *et al.*, The GPI-anchored protein COBL11 is necessary for regulating pollen tube integrity. *Cell Rep.* **42**, 113353 (2023).
54. Y. L. Zhou *et al.*, The tip-localized phosphatidylserine established by *Arabidopsis* ALA3 is crucial for Rab GTPase-mediated vesicle trafficking and pollen tube growth. *Plant Cell* **32**, 3170–3187 (2020).